Diffusion of fluids confined in carbonate minerals: a molecular dynamics simulation study for carbon dioxide and methane-ethane mixture within calcite

Marcelle B. M. Spera[a,b], Flávia N. Braga[a], Rodrigo A. C. Bartolomeu[a], Ioannis G. Economou[b], Luís F. M. Franco[a,*]

[a] *School of Chemical Engineering, University of Campinas, Av. Albert Einstein 500, CEP:13083-852, Campinas, Brazil*
[b] *Chemical Engineering Program, Texas A&M University at Qatar, P.O. Box 23874, Doha, Qatar*

Abstract

The ability to calculate how different compounds diffuse within microporous structures is paramount for a number of applications in the oil & gas sector, from oil exploration to separation, and even for the design of Carbon Capture, Utilization, and Storage (CCUS) processes. Molecular Dynamics simulations entail an excellent alternative to cases for which an experimental determination is unfeasible or extremely difficult, as it happens for fluids in micropores. Nonetheless, being confined within a mineral micropore makes the fluid spatial distribution inhomogeneous, requiring appropriate methods to compute the diffusion coefficients. Recently, some of us presented a new method for this purpose (Franco *et al. J. Chem. Theory Comput.*, 12, 5247-5255, 2016). In this work, we present a detailed study on how to apply such a method exploring fluids confined within calcite walls, which is a mineral representative of carbonate rocks found in several geological formations. From our results, we were able to map the evolution of the self-diffusion tensor components throughout the pore, showing the anisotropy among the components at different directions. We also show the influence of confinement and observe a significant effect at the center of the pore for small micropores (< 7.5 nm), where the density distribution is constant. This is an unexpected result that shows how the confinement effect is manifested even at the so-called "bulk-like" region at the center of the pore.

Keywords: confined systems, self-diffusion tensor, calcite micropores, natural gas, CO_2

*Corresponding author
Email address: lmfranco@unicamp.br (Luís F. M. Franco)

1. Introduction

Diffusion coefficient is an important transport property of fluids with applications in adsorption-based separations, membrane technologies and gas exploration, among others [1, 2, 3, 4, 5]. This transport property is a measure of the average displacement of a molecule from its initial position in a system, and can be computed from the self-diffusion of particles - molecular motion without the presence of a chemical potential gradient or external forces [6, 7, 8]. It is well-known that confinement affects fluid properties, including diffusion. The determination of this transport property for fluids within microporous structures has a great impact in a number of applications to the oil & gas sector, from exploration to separation, and even to the design of Carbon Capture, Utilization, and Storage (CCUS) processes [9, 10, 11, 12, 13].

In the case of an inhomogeneous fluid, the diffusion coefficients depend on the direction in which they are measured [14]. When confined, the motion of particles are bounded by the confining region, with different diffusion coefficients in different regions [15]. The equilibrium spatial distribution of particles is nonuniform, hence methods derived from the traditional diffusion equation neglecting density spatial variations are unsuitable.

For the cases where the confining space is small enough to affect fluid particle distribution, we have to take into account the interaction of the particles with the walls. This interactions affects not only diffusion, but properties of confined fluids at equilibrium [16, 17, 18] and at non-equilibrium conditions [19]. Although at the center of the pore there might be a region with "bulk-like" behavior, near the surface, a density peak with huge influence of the confining material and a couple of extra layers that are still under strong influence of the walls regarding fluid transport emerge [5]. Isolating different contributions to molecular diffusion experimentally can be very difficult, especially when com-

plex systems and extreme conditions are involved. Moreover, challenges also emerge in the theoretical predictions of the properties as a result of the lack of knowledge on the confinement effects. Classical Molecular Dynamics (MD) simulations entail a set of numerical techniques that enable a deeper assessment of these systems by studying their dynamical behavior with atomistic resolution, simulating the time evolution of molecules from classical models of their interactions [20].

A system where the diffusion under confinement shows interesting behavior is n-alkanes and CO_2 confined within calcite micropores. This environment is present in shale and tight reservoirs, since calcite is the most stable polymorph of carbonate rocks - the major component of natural gas reservoirs in the Middle East [21], and other regions [22, 23, 24]. The knowledge of properties of fluids confined within this mineral is important for reducing carbon footprint of oil and gas industry and enhance oil recovery [25, 26, 27, 28, 29]. Using molecular simulation, Franco et al. [30] showed that, near surface of the calcite mineral, an anisotropy among the parallel components of the self-diffusion tensor due to the structure of the calcite mineral is found. The presence of void spaces in the mineral surface allows particles to diffuse faster at one of the parallel directions than the other. This behavior was observed for pure CH_4, pure C_2H_6, pure N_2, pure CO_2, and CH_4/C_2H_6 binary mixtures [30, 31, 32]. Santos et al. [33] studied the interaction of aqueous electrolyte solutions with calcite walls, focusing on enhancing oil and gas recovery processes using water flooding. They reported wettability changes for the calcite and influence of confinement on the ionic conductivity. The impact of enhanced gas recovery technologies was also approached by other authors [34, 35], evaluating the effect of CO_2 and H_2O on shale gas within calcite micropores.

Calcite is also present in many geological formations considered as potential

candidates for geological carbon sequestration, that is, long-term storage of carbon-dioxide in deep saline aquifers [36]. Interaction of CO_2 with mineral phases is crucial to estimate storage capacity and to determine potential leakage to the surface [37]. Striolo and co-workers evaluated by molecular simulations the contact angle of CO_2 with the calcite wall to see the effect of the wettability [38] and the presence of impurities such as ethanol [39]. Due to its importance to the energy sector and to a more sustainable future, adsorption and diffusion properties of CO_2 confined within calcite pores have been studied by several authors [40, 41, 42, 43].

Modeling diffusion and understanding the confinement effects on it is crucial to describe diffusion-driven or limited processes. In this work, we take a deeper look at the calculation of self-diffusion for confined systems (slit-pore) from MD simulation data. We compute the self-diffusion profile throughout the pore, the confinement effect at the central region of the pore, and explore the application of the method to systems within calcite micropores.

2. Simulation details

We simulated two systems confined between two parallel plates of calcite: (i) equimolar binary mixture of methane and ethane and (ii) pure CO_2. The calcite plane considered was $\{10\bar{1}4\}$ orthogonal to the z direction with xyz dimensions of 4.990 nm x 4.856 nm x 1.212 nm. The pore size was fixed as $H = 3.5$ nm along the z axis, unless otherwise specified. All systems were simulated at 375 K and had overall density of 250 $kg{\cdot}m^{-3}$. At these conditions, CH_4, C_2H_6, and CO_2 are at a supercritical state when unconfined.

Classical MD simulations were performed with GROMACS 5.0.2 [44], using the Leap-Frog algorithm with a time step of 2 fs for the numerical integration of the equations of motion. A velocity-rescale thermostat [45] with relaxation

time $\tau_T = 1.0$ ps was used to control the temperature of the system. We applied periodic boundary conditions to all directions, without tail corrections due to the inhomogeneity of the systems [46, 47].

Each system was equilibrated in the canonical ensemble for 20 ns followed by 50 ns of production time in the same ensemble. Positions and velocities were stored every 0.2 ps. The final trajectory was divided in 5 blocks of 10 ns each to calculate the standard deviations of self-diffusion coefficients.

2.1. Finite-size effect corrections for bulk diffusion coefficients

For comparison, simulations of unconfined fluids were performed. In those cases, finite-size effect corrections, due to the spurious hydrodynamics induced by the periodic boundary conditions, were applied to the diffusion coefficients using Yeh and Hummer [48] method. These corrections require the medium viscosity, and simulations of bulk fluids to calculate this property were performed with LAMMPS [49, 50] using the Velocity-Verlet algorithm with a time step of 2 fs. Equilibration and production phases were executed at the canonical ensemble for 20 ns and 10 ns respectively. The Nosé-Hoover thermostat implemented by Shinoda et al. [51] was used with damping parameter of 1 ps. Viscosity was obtained with the Green-Kubo approach [52, 53] considering the time integral of the stress auto correlation function, with correlation length of 1.5 ps and sample interval at every simulation time step.

2.2. Force Fields

To model CH_4 and C_2H_6, we used the the Transferable Potential for Phase Equilibria (TraPPE) force field developed by Martin and Siepmann [54]. Unlike fully atomistic representations, such as the OPLS-AA force field from Damm et al. [55], TraPPE force field implicitly accounts for hydrogen atoms by using a United-Atom approach. United-Atom representation of molecular fluids reduces

substantially the computing time without loss of accuracy in the calculations of physical properties. TraPPE force field was also applied for CO_2 [56], describing carbon dioxide as a rigid three-site model. This is a well established force field that accurately predicts equilibrium and transport properties of hydrocarbons and CO_2, as is shown by Aimoli and co-workers [57, 58, 59].

Calcite mineral interactions were described by the force field proposed by Xiao et al. [60]. This force field is one of the many descriptions of calcite minerals, among force fields proposed by Pavese et al. [61] and Raiteri et al. [62], for example. The force field of Xiao et al. [60] captures the elastic properties of the calcite mineral, is transferable for similar minerals, such as aragonite, and was developed based on the Lennard-Jones potential, which is the same potential used for TraPPE force field. We set a cutoff radius of 1.0 nm for non-bonded interactions. The electrostatic interactions were computed using the Particle Mesh Ewald method [63]. Cross potential parameters for fluid-wall interactions were computed from geometrical combining rules.

3. Self-diffusion under confinement

In the case of an inhomogeneous fluid, methods to calculate the components of the self-diffusion tensor considering the break of symmetry due to the confining walls should be employed. Instead of Fick's phenomenological equation, a more suitable approach would be methods based on the Smoluchowski equation (Eq. 1). This equation describes the time evolution of a particle's density and is a generalization of the diffusion equation for the case where there is an external force acting on the particles [64, 65]:

$$\frac{\partial p(\mathbf{r},t)}{\partial t} = \boldsymbol{\nabla} \cdot \mathbf{D} e^{-\beta W(\mathbf{r})} \cdot \boldsymbol{\nabla} \left[e^{\beta W(\mathbf{r})} p(\mathbf{r},t) \right], \tag{1}$$

where $p(\mathbf{r}, t)$ is the probability density function, $\mathbf{r}$ the position vector, $\mathbf{D}$ the diffusion tensor, $\beta = 1/(k_{\mathrm{B}}T)$ (k_{B} being the Boltzmann constant, and T the absolute temperature), and $W(\mathbf{r})$ is the potential of the mean force related to the density profile.

At a confined environment, there is a nonuniform particle distribution leading to different diffusion at different regions. For fluids confined within a slit pore geometry, we calculate the position-dependent components of the self-diffusion coefficient parallel to the walls following the method of Liu et al. [15]:

$$D_{||} = \lim_{t \to +\infty} \frac{\left\langle \Delta r^2(t) \right\rangle_{\Omega}}{2tP(t)}, \tag{2}$$

where $\langle \Delta r^2(t) \rangle_{\Omega}$ is the mean square displacement of the centers of mass for the particles inside the evaluated region, and the survival probability, $P(t)$, is calculated as the ratio between the number of centers of mass that remain in the layer Ω between t_0 and t, $N(t_0, t_0 + t)$, and the number of centers of mass within layer Ω at t_0, $N(t_0)$, considering multiple time origins:

$$P(t) = \frac{1}{\tau} \sum_{t_0=0}^{\tau-1} \frac{N(t_0, t_0 + t)}{N(t_0)}, \tag{3}$$

with τ being the number of time steps required for all the initial particles to leave the layer. Eqs. 2 and 3 require the particle to be in the layer for the whole time between t_0 and $t_0 + t$, and so they are functions of the whole history of this time interval and not just of the values at t_0 and $t_0 + t$ [15]. Computing these quantities, one gets profiles such as the ones illustrated in Fig. 1.

The mean square displacement for the particles that remain within the defined layer looks clearly different from the usual linear plots obtained for unbounded bulk fluids using Einstein's method. The average value for molecular motion tends to drop as particles leave the layer. Once the survival probability

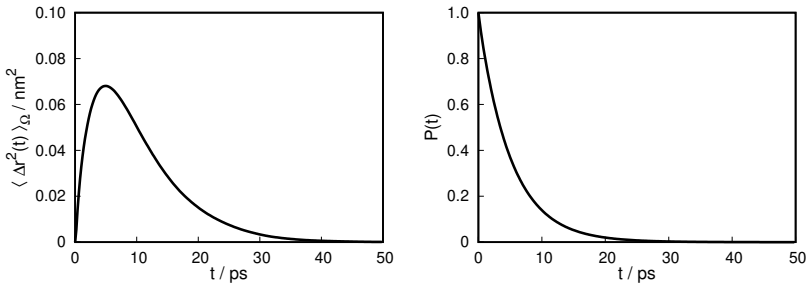

Figure 1: Mean square displacement (left) and survival probability (right) of particles of a confined fluid at a high density region near the walls. Example data for pure methane considering the motion at the direction parallel to a confining calcite slit pore.

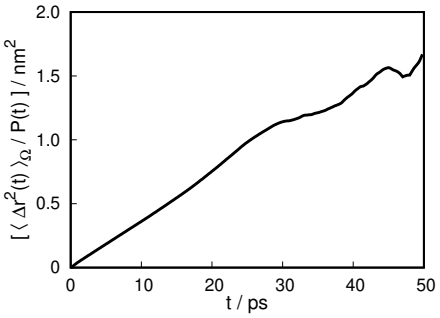

Figure 2: Mean square displacement of particles inside a layer Ω weighted by the survival probability of the particles inside such layer, allowing linear regression to calculate the self-diffusion coefficient.

is taken into account as described in Eq. 2, one gets a relation that exhibits a linear regression from which one can compute the self-diffusion coefficient (Fig. 2).

3.1. Perpendicular direction

For the calculation of the perpendicular component of the self-diffusion tensor, we used the methodology proposed by Franco et al. [46]:

$$D_{\perp} = \frac{L^2}{\alpha \tau_r}, \tag{4}$$

where L is the width of the layer Ω, α is a parameter related to the potential of mean force, and τ_r is the residence time defined as:

$$\tau_r = \lim_{t \to +\infty} \int_0^t P(t) \mathrm{d}t. \tag{5}$$

For further details on the derivation of Eq. 4, the reader is referred to the original publication [46].

3.1.1. The choice of the layer Ω

To apply the methodology of Franco et al. [46], the determination of an arbitrary layer Ω of width L where the potential of mean force is linear is required for an analytical solution of the Smoluchowski equation (Figure 3). In this section, we evaluate the effect the choice of the layer interval has on the results.

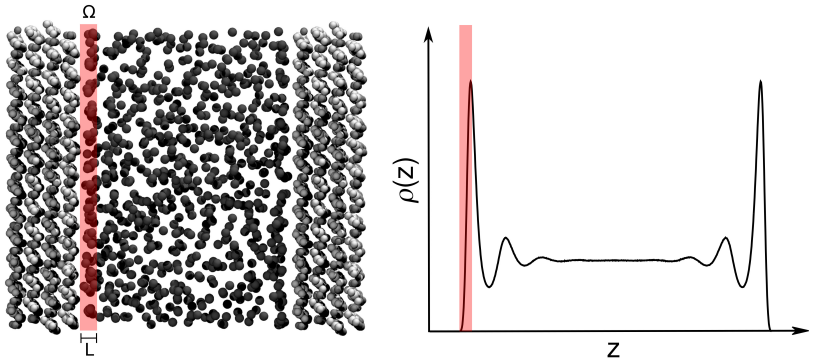

Figure 3: Layer Ω of width L chosen based on the density profile at the direction of confinement, $\rho(z)$.

We consider the higher density peak for this analysis, for which a small variation of the boundary values can highly impact the average density of the layer and hence the self-diffusion component. As an example, Fig. 4 shows the density profile of pure CH_4 confined within a calcite slit pore of aperture 3.5 nm at 375 K; highlighted, the region from 1.33 nm to 1.39 nm, corresponding to

the beginning of the first density peak on the left side. The local density goes from zero to higher than 200 kg·m^{-3} within this small 0.06 nm range.

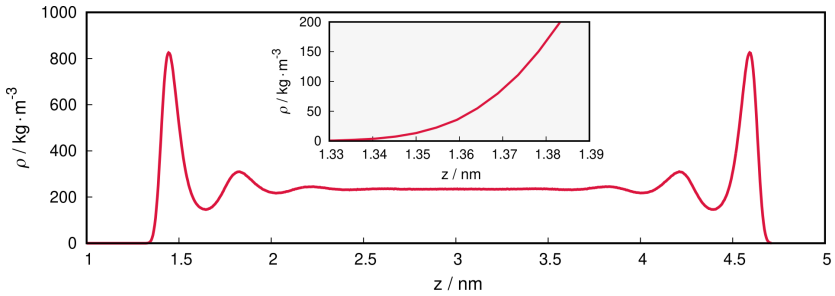

Figure 4: Density profile of pure CH_4 confined within a calcite slit pore of 3.5 nm at 250 kg·m^{-3} and 375 K. The inset plot shows a zoom view of the beginning of the first high density peak.

Now, we analyse how the parameters for the perpendicular component of the self-diffusion change depending on the region considered. By changing the lowest boundary value of the region ($z_{\min}$) and keeping the end boundary the same (the top of the peak), we follow how the α parameter from Eq. 4 behaves and how it reflects on the value of the perpendicular self-diffusion, $D_{\perp}$ (Fig. 5). The expression to calculate α is shown in Eq. 6.

$$\alpha^{-1} = 4\omega L \frac{(e^{\omega L}+1)}{(e^{\omega L}-1)} \sum_{\mathrm{j}=0}^{+\infty} \left[(2j+1)^4\pi^4 + \frac{3\omega^2 L^2}{4}(2j+1)^2\pi^2 - \frac{\omega^4 L^4}{4} \right]^{-1}, \quad (6)$$

where ω is related to the potential of mean force ($\beta W(\mathbf{r})$ from Eq. 1). The value of α was obtained considering the perpendicular self-diffusion coefficients constant within the layer $[0, L]$, and that the initial condition to solve Smoluchowski equation is given by the equilibrium density distribution of the fluid within the pore (its full derivation can be found in the original work [46]). Different initial conditions correspond to different expressions for α. Recently, Heijmans et al. [66] have solved the Smoluchowski equation using a similar procedure, but con-

sidering a Dirac delta function as the initial condition, which results, at least numerically, in a different value of α for bulk fluids than the one expressed in Eq. 6.

The layer Ω is assumed to be sufficiently small so one might consider a linear potential described by the relation:

$$-\beta W(r) = \ln \rho(r) = \omega r + \xi, \tag{7}$$

with ξ a constant independent of the position. Hence, ω is obtained by finding the slope of the logarithm of the density, $\ln \rho(r)$, with respect to the position r.

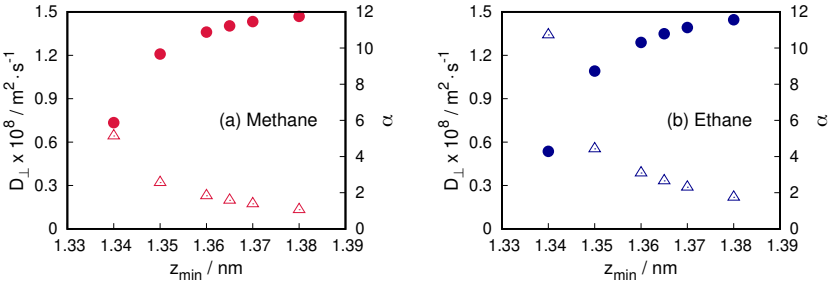

Figure 5: Impact of the initial boundary value of the region Ω on the calculation of the perpendicular self-diffusion: triangles (△) for $D_\perp$ and filled circles (•) for α. The values were calculated for pure components confined within calcite slit pores of 3.5 nm at 375 K.

As we increase the lower boundary value for the layer, the value of α gets closer to 12. As it has been proven in the original article [46], $\alpha = 12$ for homogeneous systems, *i. e.*, systems with a constant density profile within the selected layer, considering the initial condition to solve the Smoluchowski equation as the equilibrium density profile. Depending on the chosen lower value for the boundary, we have a different $D_\perp$. This is a direct consequence of the layer average density: for higher densities, we get lower diffusion coefficients, as can be seen in Table 1. As we increase the value of $z_{\min}$, the average density of the selected layer increases, and hence the perpendicular self-diffusion coefficient decreases. The parallel components remained fairly constant with the different

boundary values, changing only up to 5%. Nevertheless, despite the observed variations, an anisotropy between $D_{||}$ and $D_{\perp}$ for all cases is observed, with the latter always having a smaller magnitude.

Table 1: Perpendicular self-diffusion coefficient dependency on layer size and density. Data for pure components confined within calcite slit pore. The units are: $z_{\min}$ (nm), L^2 (nm^2), ω (nm^{-1}), $\rho \pm 0.01$ (kg·m^{-3}), and $D_{\perp} \pm 0.3\%$ (m^2·s^{-1}).

	$z_{\min}$	L^2	ω	ρ	$D_{\perp} \times 10^8$
Methane	1.340	0.0110	48.275	386.13	0.642
	1.350	0.0090	38.363	442.34	0.320
	1.360	0.0072	32.633	487.36	0.229
	1.365	0.0064	30.003	512.07	0.198
	1.370	0.0056	27.517	538.11	0.173
	1.380	0.0042	22.754	593.24	0.133
Ethane	1.340	0.0139	46.301	439.79	1.341
	1.350	0.0117	38.009	498.38	0.553
	1.360	0.0096	33.092	545.08	0.386
	1.365	0.0086	30.753	570.83	0.332
	1.370	0.0077	28.514	598.14	0.288
	1.380	0.0061	24.226	656.83	0.219

3.1.2. Extension to mixtures

We have previously shown [32] that the anisotropic behavior is also present in confined binary mixtures. To apply this method to calculate self-diffusion coefficients of fluid mixtures, we consider each of the density profiles separately. This means that each component may have layers Ω of different sizes L. As we have shown in the above sections, the choice of layer boundaries can affect the results. For consistent evaluation and reliable results, we choose a layer that has the same physical behavior based on the density profile, i.e., containing the whole high density peak or in a linear density region for example, regardless if the boundaries values are slightly different. Figure 6 illustrates this choice for a confined mixture of ethane and methane. For the calculation of the perpendicular diffusion component, only the first half of the high density region is considered to comply with the requirement of a linear potential of the mean

force.

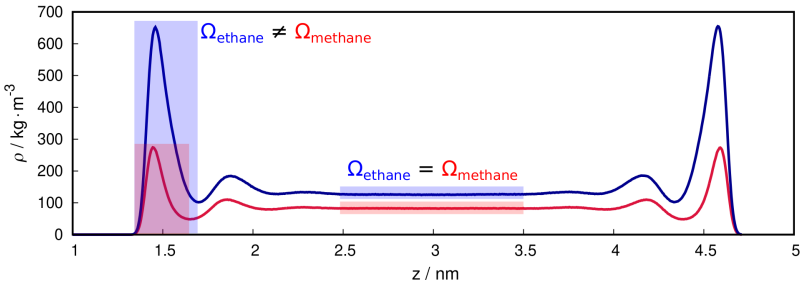

Figure 6: Choice of layers to calculate the self-diffusion tensor for mixtures: areas comprising the high density region and areas with a constant density. Data for a confined mixture of methane (red) and ethane (blue) within a calcite slit pore of 3.5 nm with overall density of 250 kg·m^{-3} and 375 K.

When dealing with multicomponent mixtures, one must account for the cross-interactions to consider how the components affect each other. While self-diffusion captures the Brownian motion of molecules, and can even be used to compute the viscosity of the mixture [67], correlation effects are better described by the calculation of the Maxwell-Stefan diffusion coefficient [68, 69, 70]. However, the calculation of Maxwell-Stefan diffusion for confined fluids is not straightforward [71, 72, 73] and will not be addressed in this study.

4. Results and discussion

4.1. Diffusion of confined CO_2

The dynamic behavior of CO_2 confined within calcite has significant potential implications for carbon storage in geological formations [74, 75, 76, 77, 78, 79]. CO_2 has a strong interaction with this mineral, which makes the calculation of the perpendicular self-diffusion coefficient close to the walls challenging when using the method of Franco et al. [46] as a consequence of the very sharp density profile. As previously mentioned, to apply the method, the choice of a layer Ω where the density profile is linear is required. For CO_2-calcite systems,

the linear region of the potential of the mean force at the high density peak near the wall is too small, without sufficient centers-of-mass remaining within the layer long enough to calculate their self-diffusion coefficient.

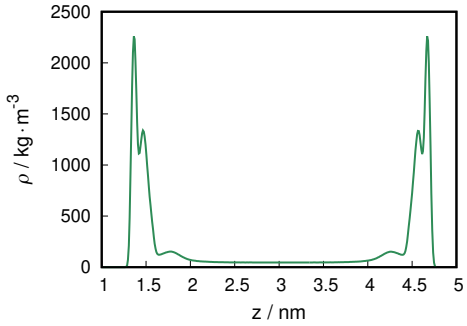

Figure 7: Density profile for CO_2 confined within calcite pore 3.5 nm wide with a global density of 250 kg·m^{-3} at 375 K.

From the density profile (Fig. 7), the strong interaction between CO_2 and calcite can be observed, with preferential adsorption on the calcium sites, as previously reported by some of us [25]. The strong adsorption on the calcite walls results in a central region with average constant density much lower than the global value of 250 kg·m^{-3}.

To assess the self-diffusion behavior, we look at this central region for slit pores with different distances between the surfaces. Simonnin et al. [80] reported that slit pores with a width/height ratio greater than 2.8 present considerable finite-size effects. Following their suggestion, and based on the xy width of our calcite mineral, we considered pore sizes from 3.5 up to 12.5 nm. Table 2 summarizes the chosen regions for each pore and gives an overview of the parameters for each case. The density ρ_{bulk} is the input density of the bulk simulations, based on the average density of the central region for the corresponding pore size. We have computed the self-diffusion of bulk fluids using Einstein's method (based on mean square displacement) and applied finite-size effects corrections using Yeh and Hummer [48] method.

Table 2: Values of z (nm) and average density (kg·m^{-3}) of the layer for the calculation of the self-diffusion tensor components at the center of the pore. Self-diffusion coefficient of unconfined fluid at local density (D_{bulk}), average self-diffusion coefficient at parallel direction ($D_{||} = {}^{(D_{xx}+D_{yy})}/_{2}$, and $^1/_3$ of the self-diffusion tensor trace (**Tr**). Diffusion values are in $\times 10^8$ m^2·s and subjected to standard deviation up to 6%. Data for pure CO_2 at 375 K.

Pore size (nm)	z_{min}	z_{max}	ρ_{bulk}	D_{bulk}	$D_{||}$	$^1/_3$**Tr**
3.5	2.5	3.5	45	50.0	32.9	22.6
5.0	3.0	4.5	94	28.1	24.1	17.1
7.5	3.0	7.0	140	22.7	17.3	13.7
10.0	3.0	9.0	165	15.5	15.2	12.7
12.5	3.0	11.0	182	14.5	14.2	12.3

For confined CO_2, the tensor trace and the self-diffusion coefficients at bulk conditions are significantly different. Nevertheless, for pores larger than 7.5 nm, $D_{||}$ corresponds to the self-diffusion coefficient of the unconfined fluid at the local density (Table 2), while $D_{\perp}$ approaches the self-diffusion coefficient of the unconfined fluid at the global pore density (dashed line in Fig. 8).

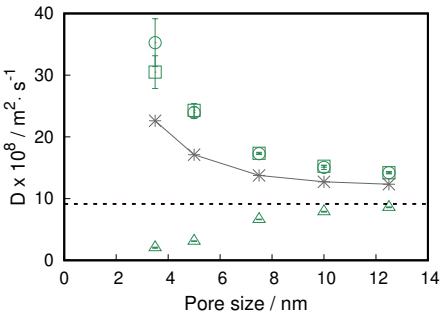

Figure 8: Self-diffusion coefficients for pure CO_2 computed at the central region with a constant density for different pore sizes. Squares (□) for D_{xx}, circles (○) for D_{yy}, triangles (△) for $D_{\perp}$, and stars (∗) for the trace of the diffusion tensor divided by three. Dashed line for the bulk value at 250 kg·m^{-3} corrected for finite-size effects.

From the results shown in Fig. 8, pores smaller than 7.5 nm are still under high influence of the confinement effect, even at the central region with constant density. This shows the importance of considering the presence of the walls acting as an external force on the system when choosing methods to compute the self-diffusion coefficient of confined fluids. Moreover, since the tensor trace varies

with the pore width, methodologies that consider a single, effective diffusion coefficient independent of the pore size may lead to an inaccurate description of the CO_2 diffusion.

4.2. Diffusion of confined CH_4-C_2H_6 mixture

Another relevant system is the confined natural gas within calcite minerals. CH_4 is the main component of natural gas, which also contains C_2H_6, N_2, and can have small amounts of heavier hydrocarbons, water, CO_2, and surfur compounds [81]. For this study, we have simulated a mixture of the lighter hydrocarbons (CH_4 and C_2H_6), two most abundant compounds of natural gas [82], to illustrate the application of the method to real systems. The self-diffusion coefficient tensor components profile for each component in an equimolar binary mixture (CH_4-C_2H_6) within a calcite micropore is shown in Fig. 9. The layer intervals selected to compute the coefficients are reported in Table 3.

Table 3: Values of z (nm) used to determine the layer for the calculation of the self-diffusion tensor components.

Layer	**Methane**		**Ethane**	
	z_{min}	z_{max}	z_{min}	z_{max}
1	1.35	1.65	1.35	1.70
2	1.65	2.10	1.70	2.12
3	2.10	2.45	2.12	2.45
4	2.45	2.75	2.45	2.75
5	2.75	3.25	2.75	3.25

Near the walls, an anisotropy between parallel components can be seen, with $D_{xx} = 1.86 \pm 0.12$ and $D_{yy} = 2.054 \pm 0.098$ for CH_4, and $D_{xx} = 1.358 \pm 0.052$ and $D_{yy} = 1.838 \pm 0.025$ for C_2H_6 (all values are in $\times 10^8$ $m^2 \cdot s^{-1}$, same as Fig. 9). The further the fluid is from the surface, the smaller the anisotropy. The confinement effect, however, still causes a difference between the parallel and perpendicular components even at the center of the pore. An increase in the self-diffusion values towards the central region of the pore is observed, with the

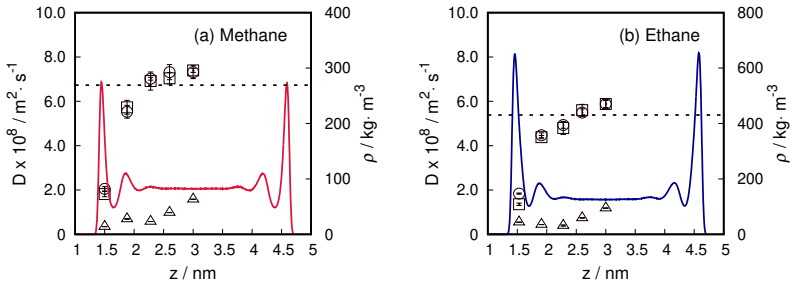

Figure 9: Evolution of the self-diffusion components throughout the pore for methane and ethane in a equimolar binary mixture with global density of 250 kg·m^{-3} at 375 K. Squares (□) for D_{xx}, circles (○) for D_{yy}, and triangles (△) for $D_{\perp}$. Dashed line for the bulk value from MD simulations corrected for finite-size effects.

tensor trace divided by three approaching the value for the unconfined fluid (dashed line).

By considering the whole region where the density is constant to evaluate the local diffusion, the effect of confinement decreases as the pore size increases, as expected. Applying the same boundary values as previously used for pure CO_2 (Table 2), we calculate the self-diffusion coefficient tensor at the center of the pore for CH_4-C_2H_6 systems (Fig. 10).

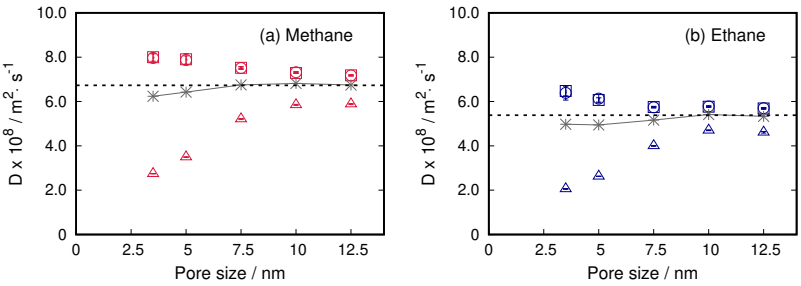

Figure 10: Self-diffusion coefficients of the equimolar mixture computed at the central region with a constant density for different pore sizes. Squares (□) for D_{xx}, circles (○) for D_{yy}, triangles (△) for $D_{\perp}$, and stars (∗) for the trace of the diffusion tensor divided by three. Dashed line for the bulk value corrected for finite-size effects.

Locally, the anisotropy between parallel and perpendicular components is observed. Nevertheless, with the average density at the center of the pore close to the global density of 250 kg·m^{-3}, the trace of self-diffusion tensor divided

by three corresponds to the value calculated through Einstein's method for the unconfined fluid at 250 kg·m^{-3} and 375 K for all investigated pore sizes, as opposed to what is observed for CO_2 confined within calcite minerals, as previously shown.

The observed behavior for the self-diffusion coefficients at the center of the pore for different pore sizes was investigated by looking into the survival probability of particles at this region (Fig. 11). The survival probability provides information about the probability of a particle to be found within the chosen layer. This must be taken into account for systems under confinement since the density distribution within the pore is nonuniform, hence the particle behaves differently depending on its position and cannot be represented by the average behavior at the hydrodynamic limit.

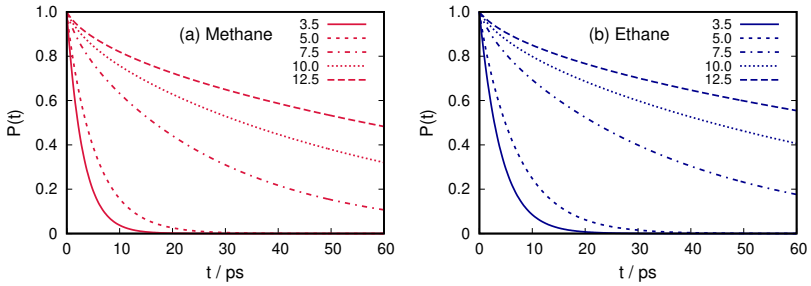

Figure 11: Survival probability evolution with time. For tighter pores, the particles are less likely to stay in the same layer for too long, decreasing the accuracy of the calculated properties when represented by an average behavior.

Our results show that for pores smaller than 7.5 nm there is a considerable anisotropy between parallel and perpendicular self-diffusion at the central region of the pore with constant density for both CO_2 and CH_4-C_2H_6 mixtures confined within calcite pores. Also, the behavior of confined fluids, even at the "bulk-like" region, is affected by the confining media and care should be taken when characterizing its properties by an average behavior.

5. Conclusions

Molecular Dynamics was used to assess the methodology proposed by Franco et al. [46] to calculate the perpendicular self-diffusion coefficient by showing how the choice of parameters can influence the results. We suggest that the same layer boundary values should be considered for the calculation of $D_{||}$ and $D_{\perp}$ to correctly evaluate the results. At the center of the pore, the difference between the self-diffusion at x and y directions vanishes, and there is only a confinement effect restricting the mobility of particles at the z direction (perpendicular to confinement). This confinement effect decreases as the pore size is increased. The trace of the self-diffusion coefficient tensor remains constant for different pore widths for CH_4-C_2H_6 mixtures and is related to the self-diffusion coefficient of bulk systems at the global density. For CO_2 systems, the average parallel self-diffusion coefficient is comparable to the self-diffusion coefficient of the unconfined fluid at the local density at the center of the pore, which vary with the pore width. The perpendicular component for pores larger than 7.5 nm tends to the value of bulk self-diffusion coefficient at the global pore density. This shows how fluid interaction with confining media affects its behavior even at the center of the pore at the region known as "bulk-like", where the density profile is linear.

Diffusion-driven processes in oil and gas industry must rely on accurate estimations of transport properties to enable best performance, lower costs, and less environmental impact. The dynamic behavior of fluids is also crucial for environmental applications such as the storage of CO_2 in deep saline aquifers or in depleted oil & gas reservoirs. Computing properties of fluids under confinement is always challenging, and we have shown that adequate methods should be employed when calculating the self-diffusion coefficients of fluids confined within tight pores.

Acknowledgments

This work was partially supported by São Paulo Research Foundation (FAPESP) grant #2018/02713-8 and CNPq (The Brazilian National Council for Scientific and Technological Development). The authors thank the computer resources made available by the Center for Computing in Engineering and Science at Unicamp (FAPESP, grant #2013/08293-7), and the High Performance Computing Center of Texas A&M University at Qatar. The authors are also grateful for the financial support of the Human Resources Program of the Brazilian National Agency of Petroleum, Natural Gas and Biofuels - PRH-ANP. This publication was made possible in part by NPRP grant number 12S-0209-190064 from the Qatar National Research Fund (a member of Qatar Foundation). The statements made herein are solely the responsibility of the authors.

[1] C. R. Kamala, K. G. Ayappa, S. Yashonath, Distinct diffusion in binary mixtures confined in slit graphite pores, J. Phys. Chem. B 108 (2004) 4411–4421.

[2] S. Chempath, R. Krishna, R. Q. Snurr, Nonequilibrium molecular dynamics simulations of diffusion of binary mixtures containing short n-alkanes in faujasite, J. Phys. Chem. B 108 (2004) 13481–13491.

[3] D. J. Keffer, P. Adhangale, The composition dependence of self and transport diffusivities from molecular dynamics simulations, Chem. Eng. J. 100 (2004) 51–69.

[4] P. Krokidas, M. Castier, S. Moncho, E. Brothers, I. G. Economou, Molecular simulation studies of the diffusion of methane, ethane, propane, and propylene in zif-8, J. Phys. Chem. C 119 (2015) 27028–27037.

[5] B. C. Bukowski, F. J. Keil, P. I. Ravikovitch, G. Sastre, R. Q. Snurr, M.-O.

Coppens, Connecting theory and simulation with experiment for the study of diffusion in nanoporous solids, Adsorption 27 (2021) 683–760.

[6] R. Krishna, J. Van Baten, The Darken relation for multicomponent diffusion in liquid mixtures of linear alkanes: an investigation using molecular dynamics (MD) simulations, Ind. Eng. Chem. Res. 44 (2005) 6939–6947.

[7] M. Hopp, J. Mele, J. Gross, Self-diffusion coefficients from entropy scaling using the PCP-SAFT equation of state, Ind. Eng. Chem. Res. 57 (2018) 12942–12950.

[8] I. N. Tsimpanogiannis, O. A. Moultos, L. F. M. Franco, M. B. d. M. Spera, M. Erdős, I. G. Economou, Self-diffusion coefficient of bulk and confined water: a critical review of classical molecular simulation studies, Mol. Sim. 45 (2019) 425–453.

[9] A. Ali, A. Striolo, D. R. Cole, CO_2 solubility in aqueous electrolyte solutions confined in calcite nanopores, J. Phys. Chem. C 125 (2021) 12333–12341.

[10] L. Tao, J. Huang, D. Dastan, J. Li, X. Yin, Q. Wang, Flue gas separation at organic-inorganic interface under geological conditions, Surf. Interfaces 27 (2021) 101462.

[11] B. Kvamme, A. Graue, T. Buanes, T. Kuznetsova, G. Ersland, Storage of CO_2 in natural gas hydrate reservoirs and the effect of hydrate as an extra sealing in cold aquifers, Int. J. Greenh. Gas control 1 (2007) 236–246.

[12] G. Carchini, I. Hussein, M. J. Al-Marri, R. Shawabkeh, M. Mahmoud, S. Aparicio, A theoretical study of gas adsorption on calcite for CO_2 enhanced natural gas recovery, Applied Surf. Sci. 504 (2020) 144575.

[13] L. Tao, J. Huang, D. Dastan, T. Wang, J. Li, X. Yin, Q. Wang, CO_2 capture and separation on charge-modulated calcite, Applied Surf. Sci. 530 (2020) 147265.

[14] J. Crank, The mathematics of diffusion, Oxford University Press, 1975.

[15] P. Liu, E. Harder, B. J. Berne, On the calculation of diffusion coefficients in confined fluids and interfaces with an application to the liquid- vapor interface of water, J. Phys. Chem. B 108 (2004) 6595–6602.

[16] L. F. M. Franco, On the structure of a confined ideal gas: A statistical mechanical description with an external field, Fluid Phase Equilib. 489 (2019) 99–103.

[17] A. F. Gonçalves, L. F. M. Franco, On the conversion of the confined ideal gas distribution between the canonical and the grand canonical ensembles, Fluid Phase Equilib. 533 (2021) 112962.

[18] N. E. L. Nobre, L. F. M. Franco, Isochoric heat capacity of confined fluids: The effect of pore width, Fluid Phase Equilib. 549 (2021) 113202.

[19] M. B. M. Spera, L. F. M. Franco, The effect of thermal gradients on adsorption, Fuel 295 (2021) 120553.

[20] D. Dubbeldam, S. Calero, T. J. Vlugt, R. Q. Snurr, Molecular simulations of adsorption and diffusion in crystalline nanoporous materials, in: Handbook of porous materials: Synthesis, Properties, Modeling and Key Applications Volume 2-Characterisation and Simulation of Porous Materials, 2021, pp. 199–319.

[21] G. Berdiyorov, E. Elbashier, G. Carchini, I. Hussein, A. Sakhaee-Pour, The effect of vacancy defects on the adsorption of methane on calcite 104 surface, J. Mat. Res. Technol. 14 (2021) 3051–3058.

[22] T. F. Rexer, E. J. Mathia, A. C. Aplin, K. M. Thomas, High-pressure methane adsorption and characterization of pores in Posidonia shales and isolated kerogens, Energy Fuels 28 (2014) 2886–2901.

[23] R. Littke, D. R. Baker, D. Leythaeuser, Microscopic and sedimentologic evidence for the generation and migration of hydrocarbons in toarcian source rocks of different maturities, in: Organic Geochemistry In Petroleum Exploration, Elsevier, 1988, pp. 549–559.

[24] E. López-Chávez, A. Garcia-Quiroz, Y. A. Peña-Castañeda, J. A. Diaz-Gongora, F. de Landa Castillo-Alvarado, W. R. Carbellido, Modeling and simulation of the adsorption and storage of hydrogen in calcite rock oil fields, J. Mol. Model. 26 (2020) 1–14.

[25] M. S. Santos, L. F. M. Franco, M. Castier, I. G. Economou, Molecular dynamics simulation of n-alkanes and CO_2 confined by calcite nanopores, Energy Fuels 32 (2018) 1934–1941.

[26] A. Ali, T. T. B. Le, A. Striolo, D. R. Cole, Salt effects on the structure and dynamics of interfacial water on calcite probed by equilibrium molecular dynamics simulations, J. Phys. Chem. C 124 (2020) 24822–24836.

[27] W. Zhang, Q. Feng, Z. Jin, X. Xing, S. Wang, Molecular simulation study of oil-water two-phase fluid transport in shale inorganic nanopores, Chem. Engi. Sci. 245 (2021) 116948.

[28] S. Mohammed, G. Gadikota, The role of calcite and silica interfaces on the aggregation and transport of asphaltenes in confinement, J. Mol. Liq. 274 (2019) 792–800.

[29] F. Yan, Y. Que, M.-X. Li, Q. Wang, Molecular simulation of the adsorption

characteristics of H_2S in calcite slit-like pores, Int. J. Modern Phys. B 34 (2020) 2050169.

[30] L. F. M. Franco, M. Castier, I. G. Economou, Anisotropic parallel self-diffusion coefficients near the calcite surface: A molecular dynamics study, J. Chem. Phys. 145 (2016) 084702.

[31] T. Bui, A. Phan, D. R. Cole, A. Striolo, Transport mechanism of guest methane in water-filled nanopores, J. Phys. Chem. C 121 (2017) 15675–15686.

[32] M. B. M. Spera, L. F. M. Franco, Surface and confinement effects on the self-diffusion coefficients for methane-ethane mixtures within calcite nanopores, Fluid Phase Equilib. 522 (2020) 112740.

[33] M. S. Santos, M. Castier, I. G. Economou, Molecular dynamics simulation of electrolyte solutions confined by calcite mesopores, Fluid Phase Equilib. 487 (2019) 24–32.

[34] G. Carchini, M. J. Al-Marri, I. A. Hussein, S. Aparicio, Ab initio molecular dynamics investigation of CH_4/CO_2 adsorption on calcite: Improving the enhanced gas recovery process, ACS omega 5 (2020) 30226–30236.

[35] G. Berghe, S. Kline, S. Burket, L. Bivens, D. Johnson, R. Singh, Effect of CO_2 and H_2O on the behavior of shale gas confined inside calcite [104] slit-like nanopore: a molecular dynamics simulation study, J. Mol. Model. 25 (2019) 1–11.

[36] M. Arif, M. Lebedev, A. Barifcani, S. Iglauer, CO_2 storage in carbonates: Wettability of calcite, Int. J. Greenh. Gas Control 62 (2017) 113–121.

[37] D. Kirste, J. Pearce, S. Golding, Parameterizing geochemical models: do kinetics of calcite matter?, Procedia Earth Planet. 17 (2017) 606–609.

[38] T. T. B. Le, A. Striolo, D. R. Cole, Supercritical CO_2 effects on calcite wettability: A molecular perspective, J. Phys. Chem. C 124 (2020) 18532–18543.

[39] T. T. B. Le, C. Divine-Ayela, A. Striolo, D. R. Cole, Effects of surface contamination on the interfacial properties of CO_2/water/calcite systems, Phys. Chem. Chem. Phys. 23 (2021) 18885–18892.

[40] X. Deng, Q. Zhang, Z. Zhang, Q. Li, X. Liu, Adsorption and diffusion behavior of CO_2/H_2 mixture in calcite slit pores: A molecular simulation study, J. Mol. Liq. (2021) 118306.

[41] S. Wang, G. Zhou, Y. Ma, L. Gao, R. Song, G. Jiang, G. Lu, Molecular dynamics investigation on the adsorption behaviors of H_2O, CO_2, CH_4 and N_2 gases on calcite (110) surface, Appl. Surf. Sci. 385 (2016) 616–621.

[42] H. Sun, H. Zhao, N. Qi, Y. Li, Effects of surface composition on the microbehaviors of CH_4 and CO_2 in slit-nanopores: a simulation exploration, ACS omega 2 (2017) 7600–7608.

[43] S. Ravipati, M. S. Santos, I. G. Economou, A. Galindo, G. Jackson, A. J. Haslam, Monte Carlo molecular simulation study of carbon dioxide sequestration into dry and wet calcite pores containing methane, Energy Fuels 35 (2021) 11393–11402.

[44] M. J. Abraham, T. Murtola, R. Schulz, S. Páll, J. C. Smith, B. Hess, E. Lindahl, GROMACS: High performance molecular simulations through multi-level parallelism from laptops to supercomputers, SoftwareX 1 (2015) 19–25.

[45] G. Bussi, D. Donadio, M. Parrinello, Canonical sampling through velocity rescaling, J. Chem. Phys. 126 (2007) 014101.

[46] L. F. M. Franco, M. Castier, I. G. Economou, Diffusion in homogeneous and in inhomogeneous media: a new unified approach, J. Chem. Theory Comput. 12 (2016) 5247–5255.

[47] M. P. Allen, D. J. Tildesley, Computer simulation of liquids, 2 ed., Oxford university press, 2017.

[48] I.-C. Yeh, G. Hummer, System-size dependence of diffusion coefficients and viscosities from molecular dynamics simulations with periodic boundary conditions, J. Phys. Chem. B 108 (2004) 15873–15879.

[49] S. Plimpton, Fast parallel algorithms for short-range molecular dynamics, J. Comput. Phys. 117 (1995) 1–19.

[50] A. P. Thompson, H. M. Aktulga, R. Berger, D. S. Bolintineanu, W. M. Brown, P. S. Crozier, P. J. in 't Veld, A. Kohlmeyer, S. G. Moore, T. D. Nguyen, R. Shan, M. J. Stevens, J. Tranchida, C. Trott, S. J. Plimpton, LAMMPS - a flexible simulation tool for particle-based materials modeling at the atomic, meso, and continuum scales, Comp. Phys. Comm. 271 (2022) 108171.

[51] W. Shinoda, M. Shiga, M. Mikami, Rapid estimation of elastic constants by molecular dynamics simulation under constant stress, Phys. Rev. B 69 (2004) 134103.

[52] M. S. Green, Markoff random processes and the statistical mechanics of time-dependent phenomena. II. Irreversible processes in fluids, J. Chem. Phys. 22 (1954) 398–413.

[53] R. Kubo, The fluctuation-dissipation theorem, Rep. Prog. Phys. 29 (1966) 255.

[54] M. G. Martin, J. I. Siepmann, Transferable potentials for phase equilibria. 1. United-atom description of n-alkanes, J. Phys. Chem. B 102 (1998) 2569–2577.

[55] W. Damm, A. Frontera, J. Tirado-Rives, W. L. Jorgensen, Opls all-atom force field for carbohydrates, J. Comput. Chem. 18 (1997) 1955–1970.

[56] J. J. Potoff, J. I. Siepmann, Vapor–liquid equilibria of mixtures containing alkanes, carbon dioxide, and nitrogen, AIChE J. 47 (2001) 1676–1682.

[57] C. G. Aimoli, E. J. Maginn, C. R. Abreu, Force field comparison and thermodynamic property calculation of supercritical CO_2 and CH_4 using molecular dynamics simulations, Fluid Phase Equilib. 368 (2014) 80–90.

[58] C. G. Aimoli, E. J. Maginn, C. R. Abreu, Transport properties of carbon dioxide and methane from molecular dynamics simulations, J. Chem. Phys. 141 (2014) 134101.

[59] C. G. Aimoli, D. P. de Carvalho, P. A. Pessoa Filho, E. J. Maginn, C. R. Abreu, Thermodynamic properties and fluid phase equilibrium of natural gas containing CO_2 and H_2O at extreme pressures typically found in pre-salt reservoirs, J. Nat. Gas Sci. Eng. 79 (2020) 103337.

[60] S. Xiao, S. A. Edwards, F. Gräter, A new transferable forcefield for simulating the mechanics of $CaCO_3$ crystals, J. Phys. Chem. C 115 (2011) 20067–20075.

[61] A. Pavese, M. Catti, G. Price, R. Jackson, Interatomic potentials for $CaCO_3$ polymorphs (calcite and aragonite), fitted to elastic and vibrational data, Phys. Chem. Minerals 19 (1992) 80–87.

[62] P. Raiteri, J. D. Gale, D. Quigley, P. M. Rodger, Derivation of an accurate force-field for simulating the growth of calcium carbonate from aqueous

solution: A new model for the calcite-water interface, J. Phys. Chem. C 114 (2010) 5997–6010.

[63] T. Darden, D. York, L. Pedersen, Particle mesh ewald: An $N\cdot\log(N)$ method for ewald sums in large systems, J. Chem. Phys. 98 (1993) 10089–10092.

[64] J.-P. Hansen, I. R. McDonald, Theory of simple liquids: with applications to soft matter, Academic Press, 2013.

[65] G. Hummer, Position-dependent diffusion coefficients and free energies from Bayesian analysis of equilibrium and replica molecular dynamics simulations, New J. Phys. 7 (2005) 34.

[66] K. Heijmans, B. K. Holkenborg, S. Gaastra-Nedea, D. Smeulders, Advanced diffusion methods for H_2O in salt hydrates, Comput. Mater. Sci. 205 (2022) 111154.

[67] S. H. Jamali, R. Hartkamp, C. Bardas, J. Söhl, T. J. Vlugt, O. A. Moultos, Shear viscosity computed from the finite-size effects of self-diffusivity in equilibrium molecular dynamics, J. Chem. Theory Comput. 14 (2018) 5959–5968.

[68] X. Liu, T. J. Vlugt, A. Bardow, Maxwell–stefan diffusivities in liquid mixtures: Using molecular dynamics for testing model predictions, Fluid Phase Equilib. 301 (2011) 110–117.

[69] X. Liu, T. J. Vlugt, A. Bardow, Predictive Darken equation for Maxwell-Stefan diffusivities in multicomponent mixtures, Ind. Eng. Chem. Res. 50 (2011) 10350–10358.

[70] J. Wesselingh, R. Krishna, Mass transfer in multicomponent mixtures, VSSD, Delft, 2000.

[71] R. Krishna, J. Van Baten, Unified maxwell–stefan description of binary mixture diffusion in micro-and meso-porous materials, Chem. Eng. Sci. 64 (2009) 3159–3178.

[72] R. Krishna, The maxwell–stefan description of mixture diffusion in nanoporous crystalline materials, Microporous Mesoporous Mater. 185 (2014) 30–50.

[73] M.-O. Coppens, V. Iyengar, Testing the consistency of the maxwell–stefan formulation when predicting self-diffusion in zeolites with strong adsorption sites, Nanotechnol. 16 (2005) S442.

[74] T. Le, A. Striolo, D. R. Cole, CO_2–C_4H_{10} mixtures simulated in silica slit pores: relation between structure and dynamics, J. Phys. Chem. C 119 (2015) 15274–15284.

[75] L. Tao, Z. Li, G.-C. Wang, B.-Y. Cui, X.-T. Yin, Q. Wang, Evolution of calcite surface reconstruction and interface adsorption of calcite-CO_2 with temperature, Mat. Res. Express 6 (2018) 025035.

[76] R. Besson, M. R. Vargas, L. Favergeon, CO_2 adsorption on calcium oxide: An atomic-scale simulation study, Surf. Sci. 606 (2012) 490–495.

[77] A. Kumar, M. Noh, G. Pope, K. Sepehrnoori, S. Bryant, L. Lake, Reservoir simulation of CO_2 storage in deep saline aquifers, in: SPE/DOE Symposium on Improved Oil Recovery, OnePetro, 2004.

[78] B. Liu, C. Qi, T. Mai, J. Zhang, K. Zhan, Z. Zhang, J. He, Competitive adsorption and diffusion of CH_4/CO_2 binary mixture within shale organic nanochannels, J. Nat. Gas Sci. Eng. 53 (2018) 329–336.

[79] P. Van Cuong, B. Kvamme, T. Kuznetsova, B. Jensen, Molecular dynamics study of calcite, hydrate and the temperature effect on CO_2 transport and

adsorption stability in geological formations, Mol. Phys. 110 (2012) 1097–1106.

[80] P. Simonnin, B. Noetinger, C. Nieto-Draghi, V. Marry, B. Rotenberg, Diffusion under confinement: hydrodynamic finite-size effects in simulation, J. Chem. Theory Comput. 13 (2017) 2881–2889.

[81] J. P. Mota, Impact of gas composition on natural gas storage by adsorption, AIChE J. 45 (1999) 986–996.

[82] J. Brasili, K. Fox, D. Badamo, G. Berghe, R. Khanal, R. Singh, Molecular dynamics simulation of shale gas confined inside slit-like calcite [104] nanopore, Mol. Sim. 45 (2019) 104–110.